



Simulations of the stationary $Q = 10$ and the exit phase from the flat-top of an ITER 15MA baseline scenario: predictive JINTRAC simulation with a

Downloaded from: <https://research.chalmers.se>, 2026-04-15 06:48 UTC

Citation for the original published paper (version of record):

Eriksson, F., Tholerus, E., Corrigan, G. et al (2024). Simulations of the stationary $Q = 10$ and the exit phase from the flat-top of an ITER 15MA baseline scenario: predictive JINTRAC simulation with a consistent treatment of D and T in the whole plasma. Nuclear Fusion, 64(12). <http://dx.doi.org/10.1088/1741-4326/ad7c63>

N.B. When citing this work, cite the original published paper.

PAPER • OPEN ACCESS

Simulations of the stationary $Q = 10$ and the exit phase from the flat-top of an ITER 15MA baseline scenario: predictive JINTRAC simulation with a consistent treatment of D and T in the whole plasma

To cite this article: F. Eriksson *et al* 2024 *Nucl. Fusion* **64** 126033

View the [article online](#) for updates and enhancements.

You may also like

- [Transport and losses of energetic particles in tokamaks in the presence of Alfvén activity using the new full orbit TAPaS code coupled to FAR3d](#)
H. Betar, D. Zarzoso, J. Varela et al.
- [The onset of parametric decay of lower hybrid waves during lower hybrid current drive experiments on Experimental Advanced Superconducting Tokamak](#)
Gen Li, Taotao Zhou, Miaohui Li et al.
- [Self-consistent modelling of radio frequency sheath in 3D with realistic ICRF antennas](#)
L.F. Lu, L. Colas, L. Cao et al.

Simulations of the stationary $Q = 10$ and the exit phase from the flat-top of an ITER 15MA baseline scenario: predictive JINTRAC simulation with a consistent treatment of D and T in the whole plasma

F. Eriksson^{1,*} , E. Tholerus¹ , G. Corrigan¹, Y. Baranov¹, X. Bonnin², D. Farina³ , L. Figini³ , L. Garzotti¹ , S.H. Kim², F. Koechl^{1,2} , A. Loarte² , E. Militello Asp¹ , C. Olde¹, V. Parail¹, S.D. Pinches² , A. Polevoi² and P. Strand⁴ 

¹ UKAEA (United Kingdom Atomic Energy Authority), Culham Campus, Abingdon, Oxfordshire OX14 3DB, United Kingdom of Great Britain and Northern Ireland

² ITER Organization, Route de Vinon-sur-Verdon, St. Paul Lez Durance Cedex, France

³ Istituto per la Scienza e la Tecnologia dei Plasmi, Milan, Italy

⁴ Association EURATOM-VR Chalmers University of Technology, Göteborg, Sweden

E-mail: frida.eriksson@ukaea.uk

Received 23 January 2024, revised 26 July 2024

Accepted for publication 18 September 2024

Published 10 October 2024



CrossMark

Abstract

Designing a robust termination scenario for a burning ITER plasma is a challenge that requires extensive core plasma and divertor modelling. The presented work consists of coupled core/edge/SOL/divertor simulations, performed with the JINTRAC code, to study the $Q = 10$ flat-top phase and exit phase of the ITER 15 MA/5.3 T DT scenario. The modelling utilizes the recently implemented option to treat deuterium and tritium separately in the SOL/divertor, enabling a consistent treatment of deuterium and tritium in the whole plasma volume, which is a unique capability of JINTRAC. In addition, these are the first JINTRAC simulations of this scenario that use a first-principles transport model to self-consistently model the ECRH power deposition and to include tungsten while keeping track of tungsten sputtering and accumulation. The flat-top simulations demonstrate the possibility of sustaining a steady state fusion Q of 10 using pure deuterium gas puffs together with DT mixed pellets, which is an option to make a more effective use of tritium. Simulations of the exit phase are set up sequentially, with each phase providing initial conditions for the next, starting with a density decay at full current and auxiliary power, and demonstrate the possibility of reducing the density robustly within a few seconds. Following the density decay, a subsequent auxiliary power ramp-down in H-mode is performed with a late H–L transition at low auxiliary power, which may provide an option for the optimization of the plasma termination. The final ramp-down phase consists of a current ramp-down in L-mode to 3.75 MA.

* Author to whom any correspondence should be addressed.



Original Content from this work may be used under the terms of the [Creative Commons Attribution 4.0 licence](https://creativecommons.org/licenses/by/4.0/). Any further distribution of this work must maintain attribution to the author(s) and the title of the work, journal citation and DOI.

Keywords: ITER, integrated modelling, JINTRAC, scenario development

(Some figures may appear in colour only in the online journal)

1. Introduction

Integrated modelling is an important tool to self-consistently study the complex set of interactions occurring during all phases of the plasma discharge. To sustain optimal performance during the flat-top phase of the discharge as well as to robustly exit from burning conditions, effects such as heating, fuelling, impurity radiation and accumulation are essential. The plasma also needs to stay within operational limits, including maintaining heat loads on divertor targets below the required limits and avoiding excessive neutral beam shine-through. The simulations in this paper are performed with the integrated modelling tool JINTRAC [1], unique in its capability to self-consistently model the core/edge and scrape-off-layer (SOL)/private region (PR) in a single framework. The scenario studied is the ITER 15 MA/5.3 T DT scenario including the flat-top, fusion $Q = 10$ phase in H-mode and the subsequent termination of the discharge. The aim of the flat-top is to demonstrate the sustainment of a fusion Q of 10 using pure deuterium gas puff together with DT mixed pellets resulting in a deuterium rich plasma edge and close to a 50/50 mix of deuterium and tritium in the core for optimum fusion performance. The exit phase consists of a ramp-down of the density at full auxiliary power and current, followed by an auxiliary power ramp-down, an H–L transition, and finally, a current ramp-down in L-mode to 3.75 MA. This ramp-down scenario differs from most previous simulations, such as [2, 3] where the density is assumed to linearly drop with the current. With the inclusion of particle transport and a consistent treatment of core/edge/SOL/PR interactions, these simulations have the capability to study how fast the density decreases when the pellet fuelling is changed. Knowing the characteristic time of density decay for a given ITER fuelling system while maintaining H-mode and divertor heat load and density control will be important for robust fast-termination scenarios, and designing ramp-down simulations with magnetic control including shape control, vertical stabilization, and force limits on the coils systems. The results of the density decay rate study can also be used to set the rate for a simultaneous density and current decay scenario.

Compared to previous JINTRAC simulations of this scenario, presented in [2–4], several improvements have been made to the modelling setup including the additions of the EC code GRAY [5] to simulate the EC deposition and current drive self-consistently, the first-principle transport model EDWM [6] for anomalous core transport, the inclusion of plasma-wall interactions at the divertor and tungsten as an impurity in the plasma, and deuterium and tritium are now for the first time treated separately in the whole plasma volume [7]. The divertor heat load has been re-modelled to include contributions not only from the ion and electron particle fluxes, heat fluxes

and recombination processes⁵, but now, at run-time, with additional contributions from neutral heat loading, reflected heat, and kinetic energy ($q_{i,kin} = \rho_{m,i} v_{fluid}^3/2$), enabling improved monitoring and control. The scenario envisaged here relies on the divertor staying in a partially detached state for density control purposes, meaning a stationary divertor heat load at its peak location below 10 MW m^{-2} and strike point electron and ion temperatures above 1 eV. Accurate calculation and runtime control is therefore one essential aspect of this work.

The rest of the paper is organized as follows: In section 2 more details of the modelling setup are presented. Section 3 consists of the results of the simulations of the flat-top and section 4 the subsequent exit of the plasma from burning conditions. Finally, a summary and conclusions are given in section 5.

2. Modelling setup

2.1. Modelling workflow

Figure 1 illustrates an overview of the JINTRAC suite of codes as used in the simulations presented in this paper. It is shown that JINTRAC combines the 1.5D transport solver JETTO [8], solving the dynamical evolution of the core plasma fluid equations, and the 2D SOL/PR Braginskii fluid code transport solver EDGE2D [9]. JETTO itself is coupled to other models to include effects such as heating and particle sources from auxiliary heating and pellet fuelling, Ohmic heating and fusion reactions, current drive and diffusion, impurities, equilibrium calculations and MHD instabilities. Details of the settings and models used in this work are presented in the following subsections. EDGE2D is coupled to EIRENE [10] to enable modelling of the plasma and neutrals in the SOL/PR including gas puff and pumping, sputtering and recycling from the tungsten divertor and beryllium first wall. The simulations presented in this paper utilize the recently implemented option of treating deuterium and tritium separately in EDGE2D, resulting in a fully consistent treatment of deuterium and tritium in the whole plasma volume. As illustrated in figure 1, JETTO and EDGE2D are coupled, each providing the boundary condition to the other at the last closed flux surface. A brief description of the coupling is provided in the appendix. In the full coupling mode, both codes evolve the plasma dynamically together in synchrony with the same time step. This time step is determined by EDGE2D stability requirements and is usually less than 10 microseconds, so following the time evolution on core confinement time scales requires an excessively long wall clock time. For simulation performance, a partial core-edge

⁵ Which have been used previously in post-processing.

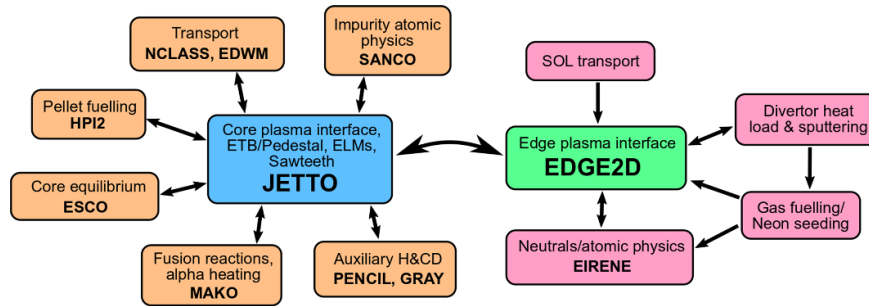


Figure 1. Flowchart illustrating the modular structure of the JINTRAC code as set up for the simulations presented in this paper.

transport coupling scheme is used allowing JETTO to advance for a maximum of 3 ms without advancing EDGE2D, followed by a 1 ms coupled phase. A correction is used to compensate for the non-conservation of particle flux during the uncoupled phase by rescaling the particle source to approximate a fully coupled run. The resulting wall clock time for the simulations presented in this paper is then on average 7 days/s when running on 6 parallel processors on the JET data centre Linux cluster. (Further parallelization is limited by the data structure design of the code.) Note that running JETTO coupled to EDGE2D/EIRENE necessitates a fixed plasma boundary which means that effects from an evolving plasma volume during the exit phase of the discharge are not included in these simulations. The free boundary equilibrium option in JETTO cannot be used when coupled to EDGE2D and modelling of coils, circuits, magnetic shape or vertical control are not included. In addition, MHD stability is assumed if within the Greenwald limit, the effects of energetic particle driven instabilities and other MHD instabilities such as NTMs are not included and the effects of sawteeth and ELMs are included though in a time averaged manner. In addition, perpendicular SOL transport is assumed, neutral-neutral collisions are neglected, momentum transport is inferred from a Prandtl number assumption, L–H transition is determined from first principles, pedestal transport is modelled with a simplified model and no reabsorption of synchrotron radiation is included.

2.2. Fuelling, impurity seeding and SOL/PR modelling

Due to the large plasma volume in ITER and high edge densities and temperatures, gas fuelling alone is insufficient to fuel the plasma. The fuelling for the $Q = 10$ ITER baseline scenario is expected to need a combination of gas puff and pellets [11]. In this paper, the fuelling scheme consists of pure deuterium gas puffs together with DT mixed pellets.

The pellets are launched from the high field side upper track, see figure 2, with velocity 300 m s^{-1} which is the maximum speed for which the pellets are expected to remain intact in ITER [12]. To model the pellet ablation and particle deposition, the HPI2 code [13] is used. The modelling assumes spherical pellets (as opposed to the cylindrical pellets which will be used in the experiment) and sizes used are 33 mm^3

(2×10^{21} atoms/pellet) in the high-density flat-top phase and a reduced 12 mm^3 (0.8×10^{21} atoms/pellet) in the low-density phase of the simulations, to reduce the density fluctuations during the pellet cycle, with a composition of 45/55 mixed DT in H-mode and pure D in L-mode. The larger pellet size corresponds to the smallest size pellets studied in [4] for the fuelling of this ITER scenario, and is in the lower range of expected pellet volumes for the ITER pellet injection system ‘nominally’ foreseen for ELM pacing but that, of course, can be used for plasma fuelling [14]. The pellet frequency is adapted by a feedback scheme to maintain a specified Greenwald density fraction ($\langle n_e \rangle / n_{\text{GW}}$ where $\langle n_e \rangle$ is the line averaged electron density and $n_{\text{GW}} = I / \pi a^2$ is the Greenwald density), the time evolution of which is shown in figure 3. The maximum change in electron density during a pellet cycle in flat-top, shown in figure 4, illustrates a pellet deposition with a peak at $\rho_t = 0.85$ (defined as the square root of the normalized toroidal flux) consistent with previous pellet modelling for this scenario, cf [4, 15].

In addition to pellets, deuterium gas puffs are used to fuel the plasma. As shown in figure 2, the gas is puffed from the upper SOL. Rates used are between $0.2 \times 10^{22}/\text{s}$ and $2.8 \times 10^{22}/\text{s}$. A higher rate helps to cool down the divertor target plates limiting the heat load to the targets, though the main technique used to avoid stationary heat load at its peak location above the maximum limit of 10 MW m^{-2} is neon seeding. Neon is injected from an inlet valve in the private region⁶, under feedback control on the maximum heat load to the target. Neon seeding with a maximum rate of $2.5 \times 10^{20}/\text{s}$ is activated when the maximum heat load exceeds 8 MW m^{-2} which subsequently radiates and cools down the target plates reducing the heat load. The neon seeding is set up like this in order to limit the risk of excessive radiation of neon in the SOL, which can lead to full detachment of the plasma. A semi-detached plasma is important for divertor heat flux control while avoiding the possibly deleterious consequences of full detachment on H-mode confinement in ITER. In addition, for numerical reasons, important molecular reactions needed to

⁶ The actual location of the neon injection is below the divertor cassette assembly, which is not represented in the JINTRAC model.

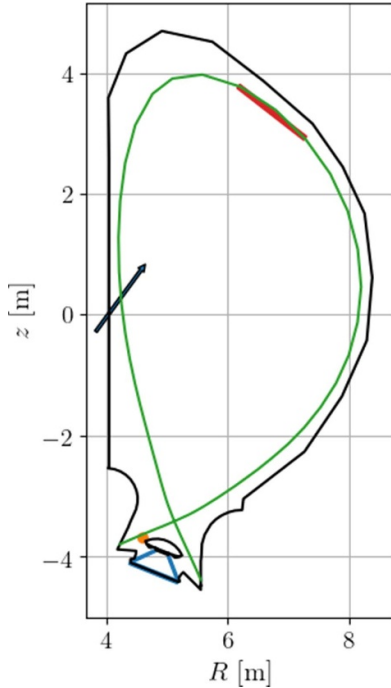


Figure 2. 2D illustration of the ITER wall, plasma separatrix (green), D gas puff location in the upper SOL (red), semi-transparent surface and pump surface with albedo = 0.99 (blue), Ne seeding in the private region (orange dot), and high field side upper pellet injector (black arrow) used in the simulation.

properly simulate detachment are not included in the neutral model used within EIRENE in these simulations and therefore the physics description of our model is only suitable for attached and partially detached conditions. Similar to previous ITER modelling with JINTRAC [3], a reduced NIMBUS-like neutral model is used instead of the full EIRENE neutral model (Kotov2008 [16] without neutral-neutral collisions and opacity, allowing the use of a source linearization scheme within EDGE2D that speeds up the simulation and makes them numerically more robust (details in appendix B of [3]). Neutral and impurity fluxes from EDGE2D-EIRENE are coupled to FRANTIC [17] and SANCO (impurity transport solver fully integrated in JETTO) respectively, at the last closed flux surface to model neutrals and impurities in the core. In addition to neon, the impurities included are helium and tungsten with reaction cross sections determined by the ADAS database [18] (year 96 for helium and neon and year 42 for tungsten). The sputtering rates are taken from the TRIM database of EIRENE [19, 20] and the atomic ionization, recombination and radiative rates are taken from the ADAS database. Zero prompt redeposition of sputtered tungsten is assumed to study the worst possible case for tungsten effects on the plasma. The particle sink consists of a pump surface below the divertor plates using an albedo of 0.99, also shown in figure 2. In the SOL, perpendicular heat and particle transport are described with radially

dependent transport coefficients. The near SOL is matched to the values at the separatrix with a gradual transition to prescribed values in the far SOL. When the value at the separatrix exceeds the prescribed value in the far SOL value (i.e. in L-mode or during ELMs) an exponential decay is used. Inter-ELM (or with continuous ELMs), when the value at the separatrix is less than prescribed in the far SOL, a barrier extends into the SOL which then rises with a tanh dependency to the far SOL value. More details and sensitivity studies of SOL transport coefficients are available in [4, 21]. Below the X-point the perpendicular transport is set to a constant. Parallel transport in the SOL is calculated from a 21-moment description with a closure allowing for arbitrary multi-species relative abundances which is necessary to be able to treat D and T separately [22]. Cross-field drifts are not included. The effect of cross-field drifts on various ITER scenarios is studied in [23] and for the partially detached conditions studied in this paper the effects are expected to be small. The main impact is expected through asymmetries in the neon distribution which would increase the asymmetry of the power density on the outer vs. inner target.

2.3. Heating and current drive

The heating scheme used consists of the originally designed heating scheme [24] of 33MW NBI (divided between two deuterium injectors at 1 MeV) and 20 MW EC in the flat-top phase of the simulation which is gradually reduced during the exit phase. To have a fast and reliable calculation of the heat and particle deposition profiles from the neutral beams the PENCIL code [25] is used. For self-consistent modelling of the EC power deposition and current drive the beam-tracing code GRAY is used. The 20 MW EC power is divided equally between the top, mid and bottom rows of the equatorial launchers in O-mode using 170 GHz. The poloidal angles are set to optimize the electron heating in the region of $\rho_t = 0.1 - 0.3$, to avoid tungsten accumulation while compensating the negative driven current from the counter direction top rows of the equatorial launcher. The resulting heat and current deposition profiles at full power in the flat-top and during the final phase of the ramp down when the total current is down to 10 MA are shown in figure 3, together with the evolution of the auxiliary power and current during the exit phase. A gradual reduction of the auxiliary power is made during the exit phase for two main reasons. First, a gradual reduction of the auxiliary power and consequently also the fusion power has been shown to limit the drop in poloidal beta, which is beneficial for vertical stability control, reducing the risk of disruption [26]. Secondly, a slower variation of the plasma stored energy helps avoid tungsten accumulation and excessive heat loads during the exit phase [27]. The NBI power is here linearly reduced to zero over 10 s and, over the same time scale, the EC power is reduced with 10 MW EC power kept between the mid and bottom equatorial launchers to help avoid full detachment [2].

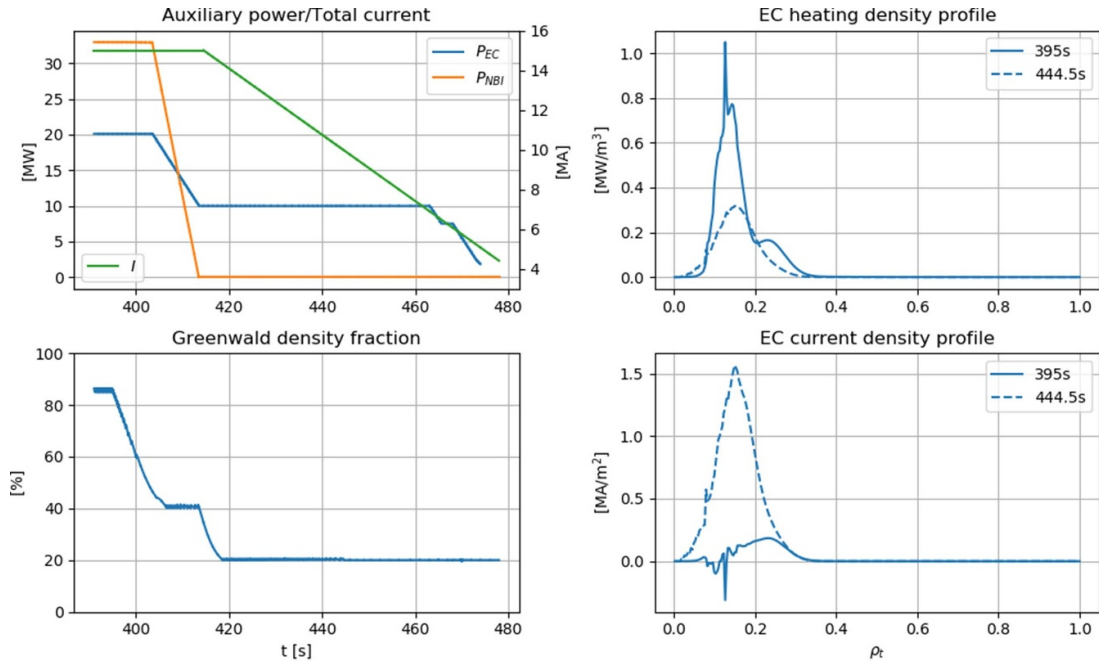


Figure 3. Evolution of the auxiliary power and total current (upper left) and Greenwald density fraction (lower left) during the flat top and all stages of the exit phase. EC heating and current deposition at the end of the flat top phase (395 s) and when total current is down to 10 MA in L-mode (444.5 s) (upper and lower right respectively).

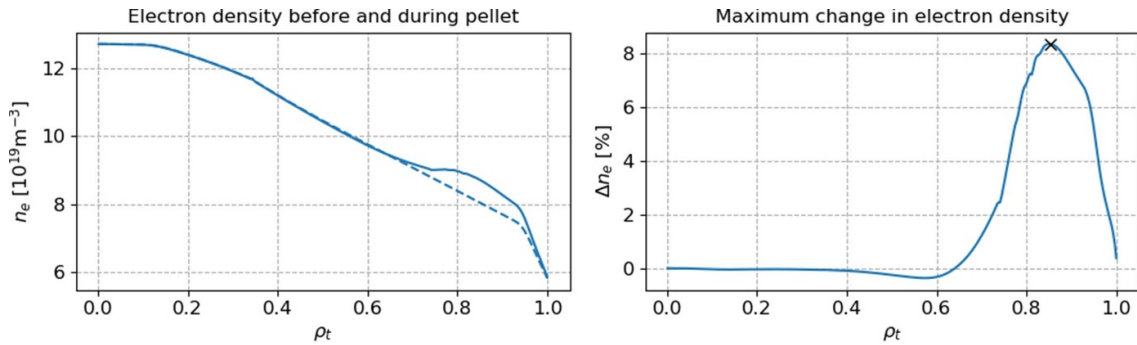


Figure 4. Electron density just before and after a pellet during flat-top (left) and maximum percentage of change in the electron density during the pellet cycle (right). The cross at $\rho_t = 0.85$ represents the peak of the pellet deposition.

A final reduction of the EC power down to zero is made when the total current is ~ 7 MA.

2.4. Core transport

For the transport in the plasma core, the neoclassical transport is modelled by NCLASS [28] and the anomalous transport is modelled with EDWM. A 10% Bohm coefficient is added, setting a lower limit on transport to provide numerical stability in regions where EDWM gives close to zero transport. In the L-mode, transport within the pedestal is dominated by the Bohm contribution, which is modelled following [29]. In addition to the improvement in its predictive capability compared to the previously used Bohm/gyro-Bohm model (which was used in the previous JINTRAC modelling [2–4]), the choice of EDWM is motivated by its resilience in simulating inverted density profiles occurring in ITER edge fuelling dominated plasmas and its computational speed. EDWM

can include an arbitrary number of ions and charge states and includes ion temperature gradient (ITG) and trapped electron (TE) mode physics in a quasi-linear fluid limit, however, detailed effects related to electromagnetic instabilities, the impact of fast particles, kinetic effects including Landau damping needs to be compared to more sophisticated nonlinear gyro-kinetic modelling for calibration and verification c.f [30] where a similar, slightly updated version of EDWM is used. In the simulations presented in this work, a scaling factor of 0.707 has been applied to the transport to keep the overall confinement close to the expected value from the confinement scaling with $H_{98,\gamma} = 1$.

2.5. MHD activity

The MHD activity included in the simulations is limited to ELMs and sawteeth. The presence of ELM control schemes is assumed so that the effect of ELMs is chosen to be time

averaged by using a continuous ELM model [31] implemented in JETTO. In the H-mode the pedestal width is prescribed as 8 cm and the pedestal transport is adjusted, with the ratio of particle to heat diffusivity set to 1, limiting the pedestal pressure gradients continuously above a specified α_{crit} resulting in a maximum pressure gradient of 2.1 in flat-top. The sawteeth is also treated in a time averaged manner for the region inside the outermost radius where the safety factor crosses the $q = 1$ surface. A time averaged profile flattening is applied in the core region inside $q = 1$ by an increase in the heat and particle diffusivity by $0.3 \text{ m}^2 \text{ s}^{-1}$ in that region, in accordance with previous JINTRAC simulations of this scenario [2].

2.6. H – L transition

For the H to L transition, we rely on scaling laws to determine the L to H power threshold, $P_{\text{L-H}}$. An H to L transition is triggered when $P_{\text{comp}} < P_{\text{L-H}}$. Within JETTO P_{comp} is set according to

$$P_{\text{comp}} = P_{\text{aux}} + P_{\alpha} + P_{\text{ohm}} - P_{\text{rad}} - \left\langle \frac{dW_p}{dt} \right\rangle, \quad (1)$$

where $\langle dW_p/dt \rangle$ is the time derivative of the stored plasma energy, time averaged over 5 ms to reduce the noise in dW_p/dt . The time average window is chosen to be large enough to avoid excessive fluctuations causing numerical difficulties and temporary back transition to L-mode while still remaining well below the confinement time so as not to affect the transition time.

To avoid an instantaneous change between suppression and non-suppression of the transport within the pedestal region in H- and L-mode respectively, a gradual change from suppression to non-suppression is set by multiplying the anomalous transport within the suppressed region by a factor $e^{-\theta/\Delta_{\text{LH}}}$, when $\theta = (P_{\text{comp}} - P_{\text{L-H}})/P_{\text{L-H}} > 0$ with Δ_{LH} set to 0.05. The power threshold scaling used is set according to the Martin scaling [32]

$$P_{\text{L-H}} = 0.0488 \langle n_{e,20} \rangle^{0.717} B_{\text{tor}}^{0.803} S^{0.941} \frac{2}{A_{\text{eff}}} \quad (2)$$

in MW, where $\langle n_{e,20} \rangle$ is the line averaged electron density in $10^{20}/\text{m}^3$, B_{tor} is the toroidal magnetic field at the geometric centre of the plasma in T, S is the plasma surface area in m^2 , and

$$A_{\text{eff}} = \frac{2 \langle n_{\text{D}} \rangle + 3 \langle n_{\text{T}} \rangle}{\langle n_{\text{D}} \rangle + \langle n_{\text{T}} \rangle} \quad (3)$$

is the effective isotope mass in a DT plasma. Note that the inclusion of a mass scaling results in a 20% reduction of the power threshold for DT plasmas compared to a pure D plasma. For ITER, the Martin scaling law is expected to be valid above the density corresponding to a Greenwald density fraction $f_{\text{GW}} = \langle n_e \rangle / n_{\text{GW}} = 40\%$ [33].

2.7. Core equilibrium

The reference ITER plasma equilibrium used in this work [34] was developed within an iterative approach of exchanging engineering and physics information obtained from the magnetic and kinetic plasma scenarios developed by using the DINA code [35]. The magnetic equilibrium inside a fixed boundary consisting of the separatrix is then calculated every 100 ms with the equilibrium solver ESCO [8] solving the Grad–Shafranov equation inside a prescribed, fixed last closed flux surface boundary with input from a prescribed magnetic field at a specified radius and a total current density profile. It includes fast ion pressure from fusion alphas (simulated with the MAKO code using alpha slowing down distribution from [36] and alpha heating power distribution between ions and electrons from [37]) and NBI with explicit smoothing of fast ion pressure profiles for numerical stability. A total current boundary condition is used for the predictive current profile calculation where the total current satisfies the current diffusion equation with contributions from an inductive current from the central solenoid together with contributions from the non-inductive current from auxiliary heating, a bootstrap current and an Ohmic current.

2.8. Summary of inputs and outputs

Inputs to the JETTO core modelling consists of initial conditions for kinetic profiles and q-profiles based on previous JINTRAC simulations of the same scenario [2] performed with simplified assumptions and deemed reasonably close to the equilibrium solutions with the improved modelling setup used in this paper. Separatrix conditions for densities, temperatures, heat and particle fluxes are taken from EDGE2D/EIRENE with the equilibrium boundary contour shape prescribed and fixed in time. Heat and particle sources from NBI and ECRH have actuator inputs for auxiliary heating power, frequency and steering angles (ECRH), energy component waveforms (NBI), and machine geometries for the EC antennas and NBI. Together with particle sources from pellets and gas fuelling, electron-ion thermal equilibration, radiation, Ohmic heating and alpha particles, particle and energy balance equations are solved for each species. Numerical parameters, such as the minimum and maximum time steps, maximum coupling intervals for JETTO-EDGE2D and grid resolutions are all provided as input to JETTO as well as specific inputs required by the individual modules coupled to JETTO.

For the SOL modelling, input to EDGE2D/EIRENE consists of a gridded magnetic geometry and a first wall 2D contour with locations of pump, gas fuelling and neon seeding sources, as shown in figure 2. The neon seeding rate is under feedback control to keep target heat loads within a prescribed limit. Cross-field transport is assumed in the form of prescribed conductivity and diffusivity chosen on the basis of modelling of existing devices. The sputtering rates are taken from the TRIM database of EIRENE and the atomic ionization, recombination and radiative rates are taken from ADAS.

The output consists of, for instance, self-consistently evolving predicted profiles of densities, temperatures, q -profiles, heating and current drive and transport coefficients. Also, core time-traces such as volume/area integrated quantities of heating and total current, local time traces such as flows across the separatrix, edge ballooning α , q_{\min}/q_{95} and average quantities such as line average density and Z_{eff} . For the SOL/PR output consists of 2D profiles of densities, temperatures, ionization/recombination rates and radiation, time traces of heat loads, divertor temperatures, gas puff rates, pump rates, sputtering yields and many more.

3. Flat-top with Fusion $Q = 10$

The flat-top phase of the simulation starts from a previous $Q = 10$ JINTRAC simulation, similar to [2], without the segregation of deuterium and tritium in the SOL or tungsten plasma-wall interactions. Using the fuelling scheme described in section 2.2 with the deuterium gas puff rate set to $1.3 \times 10^{22}/\text{s}$ results in a pellet frequency of 8 Hz when the pellets are under feedback to provide the line average density corresponding to a Greenwald density fraction of 85%. At this pellet frequency the deuterium and tritium fuelling from pellets are $0.75 \times 10^{22}/\text{s}$ and $0.9 \times 10^{22}/\text{s}$ for deuterium and tritium respectively. As illustrated in figure 5, the ion content in the core and edge are kept steady with this slightly tritium rich pellet together with the pure deuterium gas puff. The resulting total fuelling rate of $\sim 2 \times 10^{22}/\text{s}$ for D and $\sim 1 \times 10^{22}/\text{s}$ for T is well within operational limits for both the total and the tritium throughput in the ITER design [38]. Also, the combined total fuelling rate is consistent with previous JINTRAC simulations of this scenario [2] and the individual deuterium and tritium rates balance well the average flux to the pump in figure 5. The tritium fraction is 49.5% in the core and 40% in the SOL/PR due to the asymmetry of the fuelling scheme between D and T. Even with this asymmetry in the SOL/PR D vs T content, the simulations show that it is possible to sustain a fusion Q of 10. The final time trace in figure 5 consists of the confinement factor H_{98} (radiation corrected) which is 1 throughout the flat-top simulations, showing that the calculated transport is consistent with the ITER scaling law [39].

As shown in figure 6, the maximum heat load is kept just below the limit of 10 MW m^{-2} throughout the flat-top phase of the simulation using neon seeding. The neon content is subsequently tied to the heat load on the divertor targets. After 4s the level of neon saturates at 0.3% and the average neon pumped out is equal to the average of the injected and recycled neon, resulting in a radiation level of 7 MW in the core during the steady state. The total core radiation, including bremsstrahlung and synchrotron radiation is 25 MW consistent with previous JINTRAC simulations of this scenario [2].

The amount of neon will be important during the low-density, current ramp-down phase since too much neon can result in excessive cooling of the divertor plasma which can result in full detachment. Also, figure 6 shows the electron temperature at the inner and outer strike points of the divertor targets, both of which remain steady and above the 1 eV limit to avoid full detachment. In addition, the part of the divertor region where the recombination rate is higher than the ionization rate is limited to the near strike point plasma at the divertor as illustrated in figure 7. In a fully detached plasma this region would spread into the main SOL at the divertor target and not just near the strike point.

The final time traces demonstrating the steady state for this scenario are presented in figure 8. The helium level in the core saturates at 1.9% a helium source rate from fusion reactions of $2 \times 10^{20}/\text{s}$ which matches the time averaged helium pump rate. Finally, the results of figure 8 demonstrate that, in addition to maintaining acceptable divertor heat loads with low levels of neon at fusion Q of 10 (shown in figure 6), the tungsten sputtering rate and resulting tungsten radiation remain very low and there is no accumulation in the core even without any prompt redeposition of tungsten. Worth noting is that the sputtering yield is normalized to that of the main ion species in EDGE2D which is tritium in these simulations.

Profiles in the flat-top phase (at 395 s) for deuterium, tritium, helium, neon, and tungsten are presented in figure 9. The density peaking is marginally higher for tritium than deuterium, in part due to the 45/55 DT mix in the pellets which penetrates further into the core than the deuterium gas puff, and in part due to differences in transport between D and T. The pure deuterium gas puff also results in a deuterium rich edge. Ion temperature is 14.8 keV on the axis resulting in a fusion Q of 10.3 for the duration of the flat-top phase. Also shown in figure 9 are the contributions to the heating and current density and the resulting safety factor. As expected, the dominant contribution to the heating power is from the alpha heating and the total current is dominated by the inductive current with a small contribution from the auxiliary power and bootstrap current. The safety factor crosses the $q=1$ surface twice with the outermost point around $\rho_t = 0.3$. Inside this region the continuous sawtooth model is active. Worth noting is that, given the current diffusion time scale, the current density shape and corresponding q -profile, particularly on the axis where the resistivity is lowest, will be influenced by the initial condition of the previous JINTRAC simulations [3] upon which these simulations originate.

A 2D plot of the deuterium density and the ratio of tritium to deuterium density are shown in figure 10. We observe that deuterium is dominant in the far SOL as well as in the private region below the target plate. To clarify the difference between deuterium and tritium in the SOL, the density profile along the outer midplane is shown in figure 11.

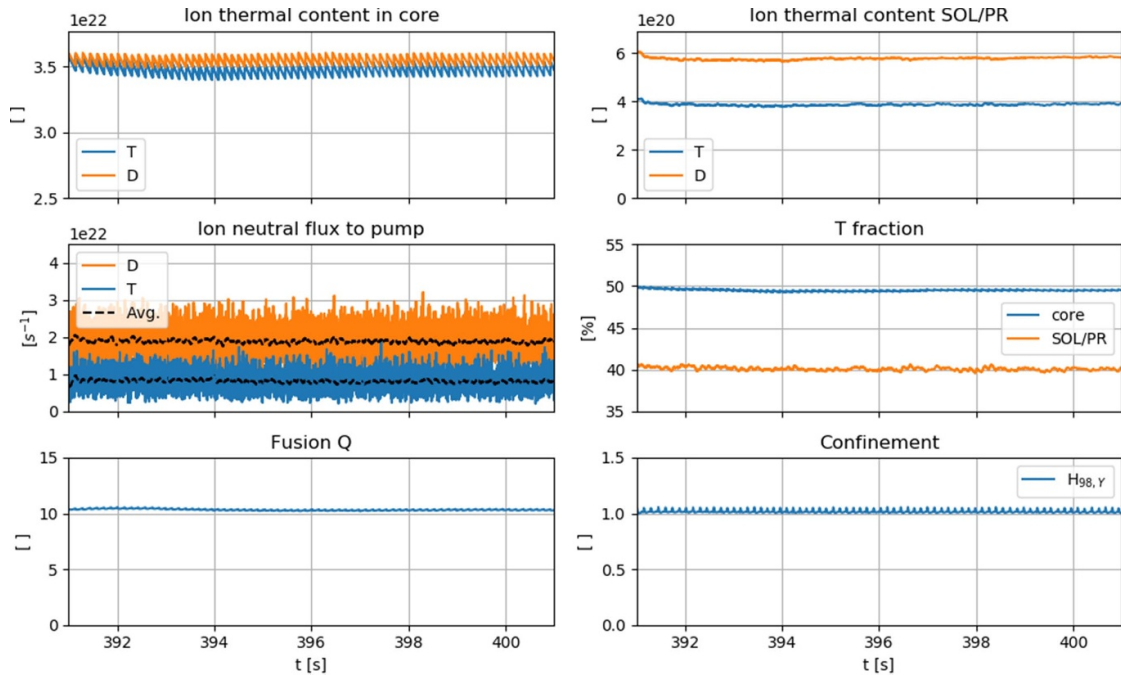


Figure 5. Time traces illustrating the steady state phase of the simulation for 45/55 DT mixed pellets and pure D gas puff. The average flux to pump for D and T is time averaged over 0.1 s.

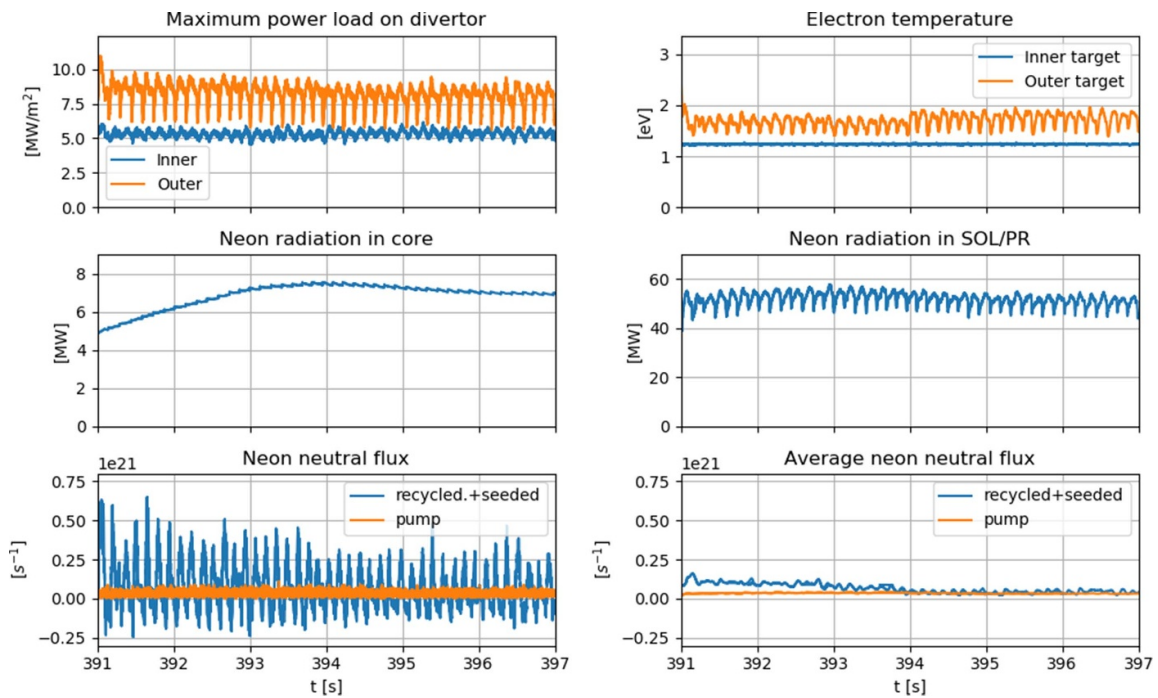


Figure 6. Time traces illustrating the steady state phase of the simulation for 45/55 DT pellets and pure D gas puff, showing the maximum heat load to the targets as well as the neon radiation in the core and SOL/PR. The neon neutral flux is time averaged over 0.05 s in the bottom right figure.

4. Exit phase

At the time of starting the simulations of the exit phase, the flat-top consisted of the initial 4 s of simulations. Therefore, the exit phase starts at 395 s with the sequential ramp down of density, power, and current.

4.1. Density decay at full auxiliary power and current

Starting from flat-top $Q = 10$ burning conditions the exit phase is initialized with a density decay at full auxiliary power and current, keeping the plasma in H-mode. During this phase the density is reduced from the flat-top density at Greenwald density fraction 85% down to 45% which reduces the fusion Q to

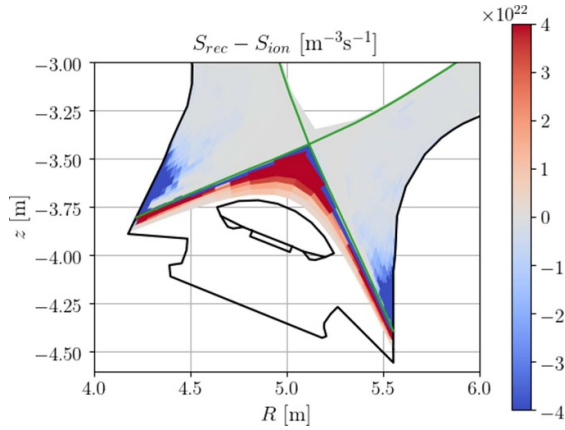


Figure 7. 2D plot of ionisation/recombination balance at 395 s including the separatrix in green and the wall contour in black. Positive values correspond to net recombination and negative ones to net ionisation.

~5. For the density decay phase, two cases are considered with summary time traces depicted in figure 12. In the first case, the pellets are instantaneously switched off and in the second a linear reduction of 5% per second of the Greenwald density fraction is specified which corresponds to an almost linear reduction of the pellet frequency from 8 Hz to 0 Hz over 5 s. As the density reduces at full auxiliary power, there is an initial increase in fusion Q associated with a short increase in fusion power, and a momentary increase in the heat load to the targets. This triggers neon seeding and there is a subsequent increase in neon in the edge and core. With the continued reduction of density, the ion temperature reduces, and the heat load is once again below the limit triggering the neon seeding, and the neon content is then steadily pumped out, reducing the content in the core and edge. There is also an increase in tungsten sputtering and the tungsten content in the core increases though from very low levels. When the density decays over a slightly longer timescale in the second case, the maximum heat load is kept below the limit of 10 MW m^{-2} , except for short spikes coinciding with the pellets. As the density is reduced at full NBI power, the NBI shine-through increases from levels of 0.05 MW at flat-top to 0.1 MW and 0.12 MW for the first and second cases respectively, which are well within acceptable levels. It is worth noting, as seen in figure 12, that the trends are very similar in the two cases and none of them result in any lasting issues in terms of radiation from tungsten in the core, excessive cool-down of the target risking full detachment or long exposure to too high heat loads. The remainder of the exit phase continues from the end of the slower density decay phase depicted in blue in figure 12.

2s into the slower density decay phase, which is the point of highest maximum heat load for the targets in this case, the heat load distribution as well as the temperatures along the target plates are shown in figure 13. At the radial location of the peak heat load both T_e and T_i are below the sputtering threshold of 5 eV and in the detachment regime range above 1 eV. Also shown in figure 13 is the 2D profile of the total impurity radiation in the SOL/PR at this time which is dominated by the

neon radiation in the divertor region. As mentioned above, this amount of neon does not lead to detachment and will gradually reduce during the remaining exit phase.

4.2. Auxiliary power ramp down at full current and H–L transition

Following the 8.5 s density decay, corresponding to the longer of the two studied cases in section 4.1, is an auxiliary power ramp-down starting at 403.5 s. As described in section 2 and illustrated in figure 14, the auxiliary power is reduced linearly over 10 s starting at 403.5 s. Pellet fuelling is used to keep the Greenwald density fraction at 40% to stay within the validity of the Martin scaling for the H–L power threshold and to limit the reduction in fusion power. With the reduction of the pellet frequency during the previous density decay, the tritium content in the core was reduced at a higher rate than deuterium which continued to be fuelled by the deuterium gas puff. The tritium fraction in the core, which was 50% during the flat-top, was reduced to 30% by the start of the auxiliary power ramp-down and remains just below 20% when the pellets are again needed to keep the Greenwald density fraction from falling below 20%. At this density and tritium fraction, the resulting H–L power threshold is around 49 MW, shown in figure 14, and the remaining fusion power and auxiliary power are high enough to keep the plasma in H-mode throughout the auxiliary power descent as intended. 7 s into the auxiliary power decrease, the edge ballooning parameter α falls below α_{crit} indicating a transition from Type I ELMy regime to ELM-free H-mode. Towards the end of the auxiliary power ramp-down at 413.3 s, when the NBI power is down to 0.6 MA and the EC power is down to 10.3 MW, $P_{comp} \approx P_{L-H}$ and the H–L transition starts. At this time, the plasma dithers between H- and L-mode for ~ 0.4 s before it transitions to L-mode and remains there for the rest of the exit phase. Profiles of the ion pressure and the ion heat and particle diffusivity are shown in figure 15 before and after the H–L transition illustrating the effect of the increase in transport at the edge in L-mode. For the heat diffusivity, the main difference between the H- and L-mode phases shown is from the change in Bohm transport, while the deuterium particle diffusivity is also enhanced in the L-mode by EDWM. The jump at $\rho_r = 0.35$ comes from the continuous sawtooth model which increases the particle diffusivity inside the outer radius where $q = 1$.

4.3. Current ramp-down in L-mode

In the final step of the exit phase, the total current is linearly reduced from 15 MA to 3.75 MA at a rate of $\sim 0.17 \text{ MA s}^{-1}$, to stay within the range of controlled plasma current ramp-down [40], at a fixed Greenwald density fraction and auxiliary power in L-mode. Following [2] and keeping some EC power throughout the majority of the ramp-down, the issue of divertor detachment is avoided. As described in section 2, pellet fuelling is used throughout all stages of the exit phase. When the total current is down to 10 MA at 445 s the pellet fuelling is turned off and deuterium gas puff alone is sufficient

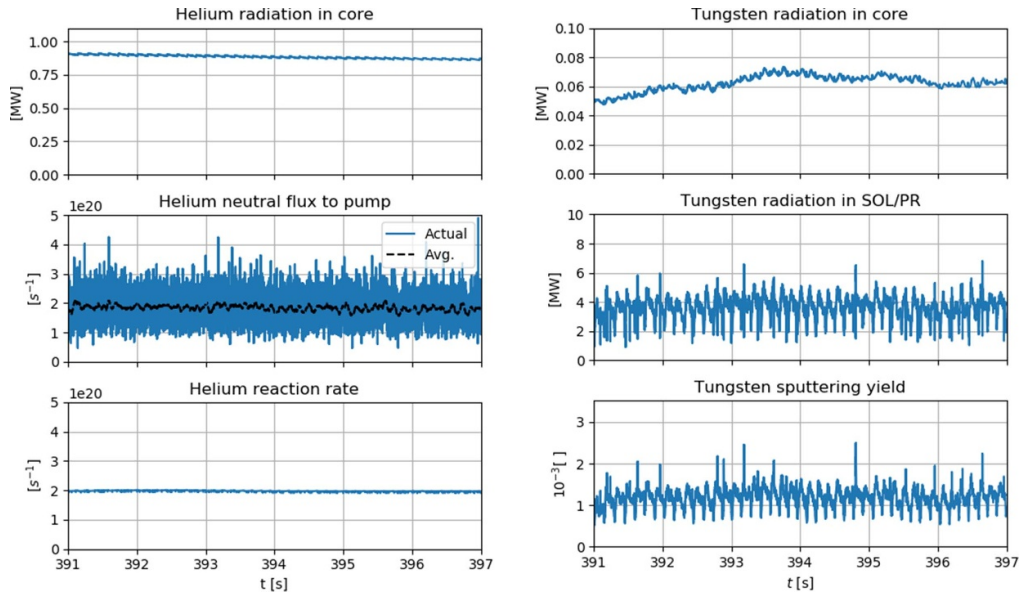


Figure 8. Time traces illustrating the steady state phase of the simulation for 45/55 DT pellets and pure D gas puff. The helium flux to the pump is time averaged over 0.05 s in the middle left plot. The tungsten sputtering yield is normalized to a main ion species which is tritium for these simulations.

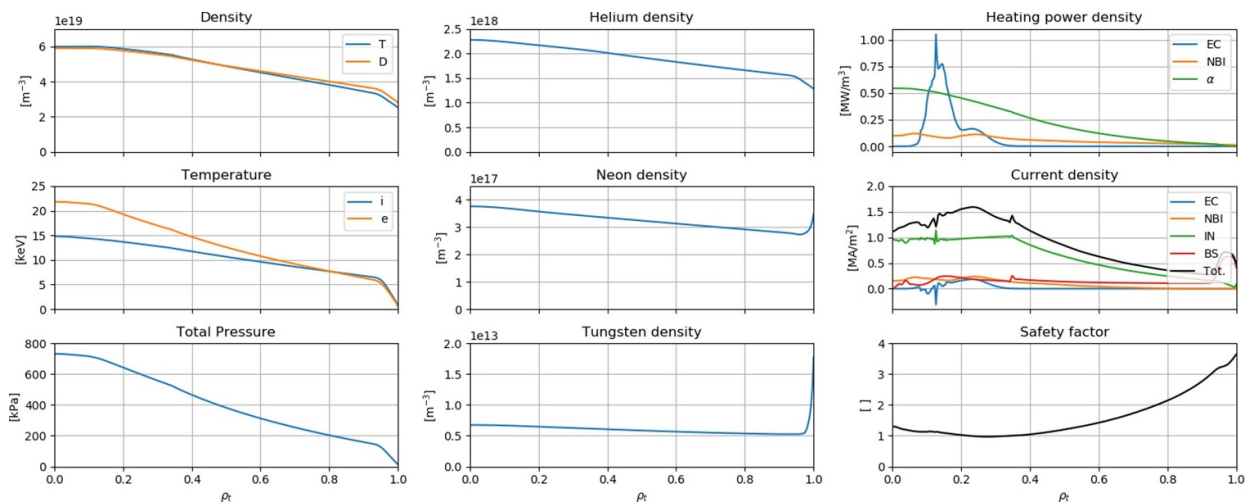


Figure 9. Core profiles at 395 s, in the flat-top phase.

to keep the density at the specified Greenwald density fraction. At this point, the tritium species, which is only a trace at this point, is removed from EDGE2D for better computational performance.

Selected time traces of the entire exit phase, including the density decay, auxiliary power ramp-down, and current ramp-down, are presented in figure 16. First of all, note that in flat-top the inductive current is about two thirds of the total current and the bootstrap current makes up the majority of the remaining current. With the reduction of density at full auxiliary power, the NBI driven current and EC driven current both increase as the bootstrap current falls. By the time the plasma is in L-mode at low density with low auxiliary power, the majority of the total current is inductive. The change in magnetic flux is shown at the last closed flux surface in figure 16 and the loop

voltage is the total corresponding to that provided by the central solenoid in addition to the PF coils and the voltage induced by the plasma. The spikes in loop voltage coincide with the magnetic equilibrium updates in ESCO. Also, worth noting is the build-up of a current hole on axis with the reduction of total current while maintaining EC power driving off-axis ECCD. The bootstrap current on the axis is very low at these low densities and the inductive current is gradually reduced on the axis. This leads to an exploding value of the safety factor on the axis and the numerical failure of the simulation due to the lack of an MHD instability model within the current hole. To limit the current hole on axis we then activate a model in JINTRAC to mimic the MHD instabilities occurring in current holes that fill in the central current. The central resistivity is increased to the value at the outer edge of the current

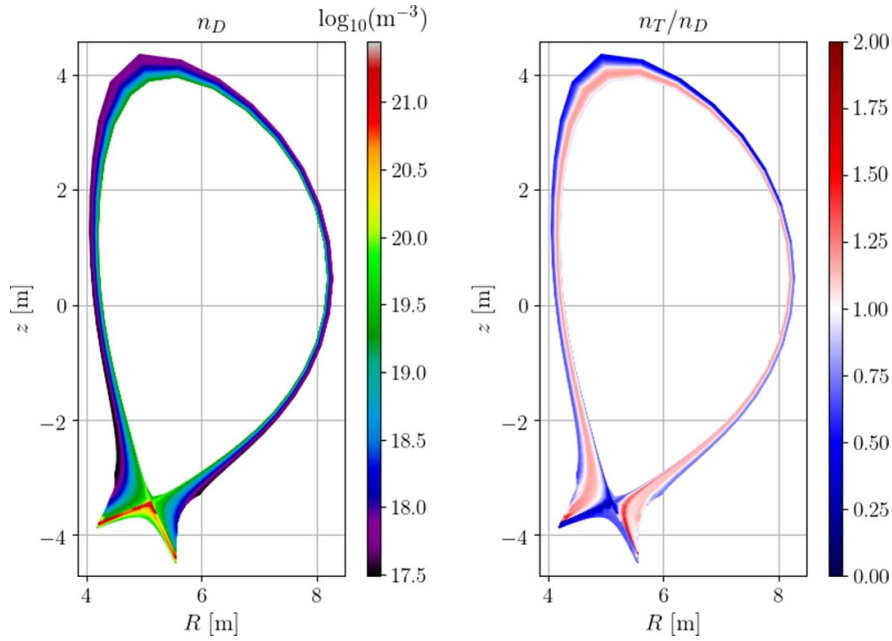


Figure 10. 2D profiles of the deuterium ion density and the ratio of tritium to deuterium density in the SOL/PR at 395 s, in the flat-top phase.

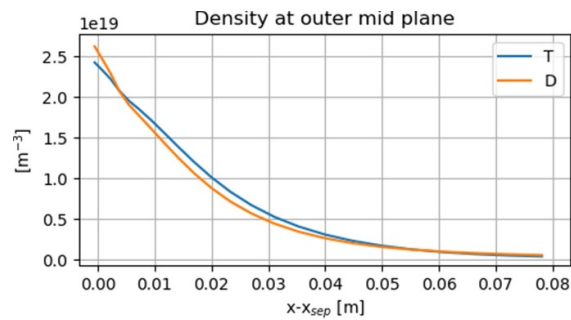


Figure 11. Deuterium and tritium density profiles along the outer midplane at 395 s. The radial grid extends slightly inside the separatrix.

hole, and this effect is clearly seen in the evolution of q_0 in figure 16 with an almost instant reduction of the safety factor along the axis. Note that removing or changing the ECCD could also be beneficial to avoid the development of the current hole. A detailed study of the ECCD including the launcher settings taking into account a decreasing plasma volume during this phase is not within the scope of this work. Finally, the plasma internal inductance increases steadily as the current is decreased. To ensure vertical stability in this phase, vertical stability and shaping control will be used in the ITER experiment, but this is not included in our fixed boundary modelling simulations. The increase in internal inductance and reduction in poloidal beta, both reduce the vertical stability margin [41], as found in previous ITER ramp-down simulations [42]. The vertical stability appears to be within the stability margin down to ~ 7.5 MA if we consider the indirect comparison with the CORSICA cases, shown in figure 17 and published in [42, 43].

However, adequate evaluation of the vertical stability cannot be achieved using fixed boundary simulations, and requires further work using a more adequate modelling tool such as DINA [35] or ITER High Fidelity Plasma Simulator (HFPS) [44].

5. Summary and conclusions

The presented work consists of the details of the sustainment of the flat-top $Q = 10$ phase and the step-wise approach for the robust termination of plasma for the ITER 15MA baseline scenario. The flat-top simulations demonstrate the possibility of sustaining a fusion Q of 10 using DT pellets and pure deuterium gas puff, which is an option to make more effective use of tritium while staying within operational limits and including plasma-wall interactions, tungsten divertor and accumulation

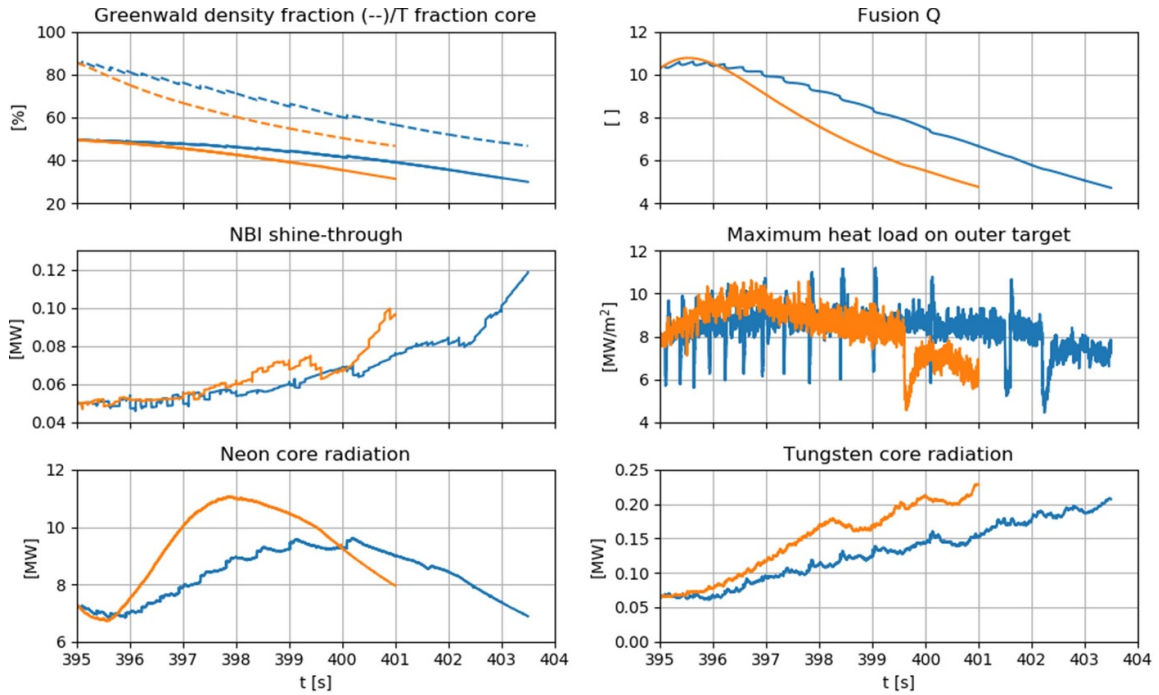


Figure 12. Time evolution during the density decay phase at full auxiliary power and current. Linear reduction of 5%–1 of Greenwald density fraction (blue) and pellet switch-off (orange).

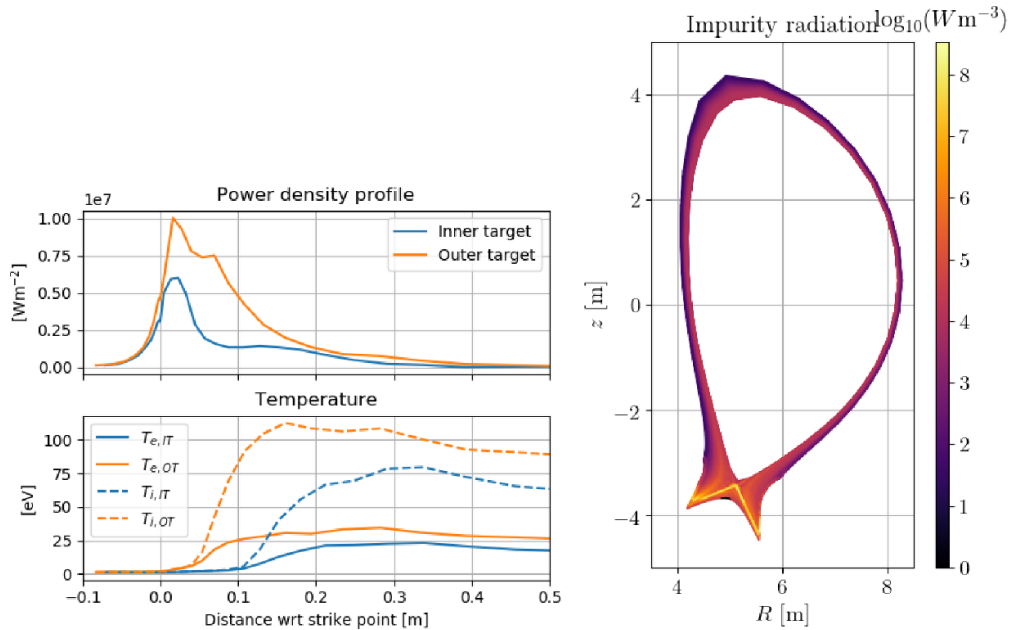


Figure 13. Power density and temperature profiles along the inner part (up until 0.5 m) of the inner and outer target at 397 s, 2 s into the density decay at full current and auxiliary power (left) when the heat load at its peak location is the highest during the density decay. 2D profiles of the total impurity radiation in the SOL/PR (right) at this time.

as well as neon seeding. Using this fuelling scheme requires that the pellet mix is slightly tritium rich to keep a 50/50 mix of deuterium and tritium in the core. The maximum heat load to the targets is kept just below the operational limit of 10 MW m^{-2} with neon seeding under feedback from the

private region. The amount of neon is saturated during the flat-top phase at a level that does not cause full detachment during the exit phase and there is no tungsten accumulation occurring. Worth mentioning is that the effect of discrete ELMs on the $Q = 10$ flat-top phase of this scenario has been shown to result

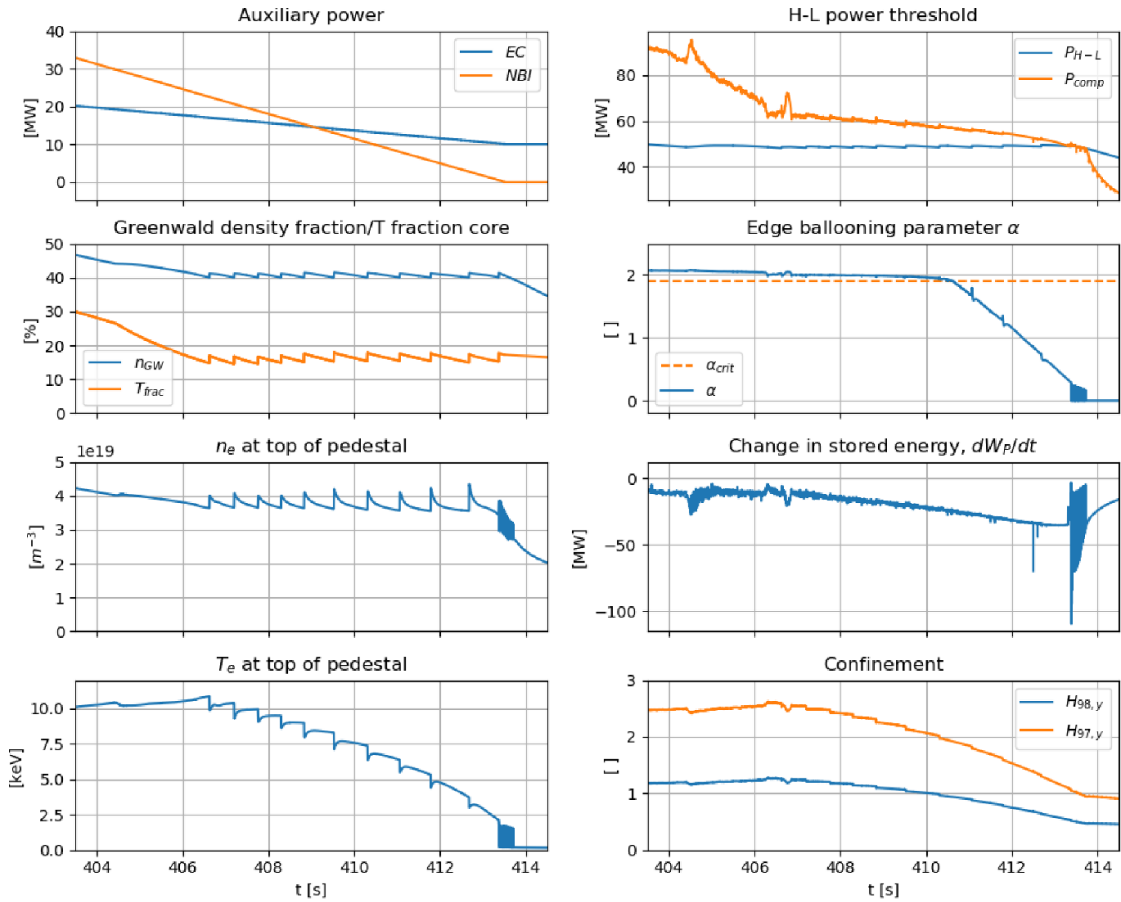


Figure 14. Time traces of the auxiliary power ramp-down starting at 403.5 s and subsequent H–L transition at ~ 413.5 s.

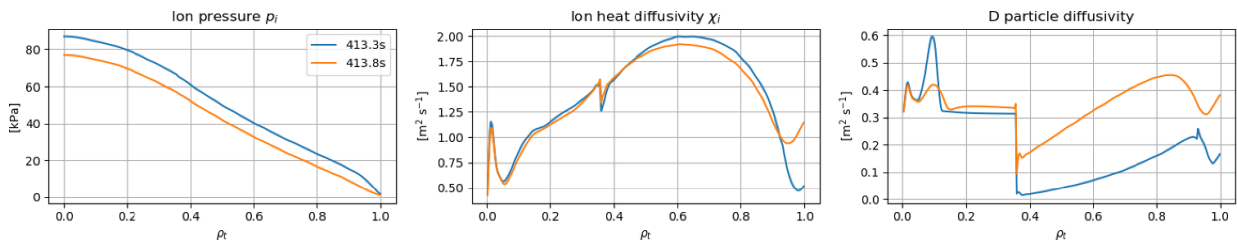


Figure 15. Profiles before and after the H–L transition.

in an increase in tungsten levels in the core and SOL/PR [45] and the impact of this on the scenario needs to be explored further in future work. An ELM mitigation system, as foreseen, may therefore be required for stable operation at high performance. The sequential setup for the exit phase consists of a gradual reduction of density at full auxiliary power and current followed by a ramp down of the auxiliary power, a late H–L transition and, finally, a current ramp down in L-mode. The density decay phase shows the promising result that the density can be reduced rather quickly. In these simulations, the density is reduced from the flat-top value of 85% Greenwald

density to 45% over 8 s without significant issues for heat load or radiation. The reduction of the pellet frequency during the density decay significantly reduces the fraction of tritium in the core, though the fusion power and remaining auxiliary power in the power ramp down phase are enough to keep the plasma in H-mode. An H–L transition occurs at the end of the auxiliary power ramp down that facilitates radial position control and vertical stability of the plasma during this transition. Finally, the total current is reduced from 15 MA to 3.75 MA in L-mode, with a change in magnetic flux at LCFS of 19Vs which is within the design constraints for ITER [46], while

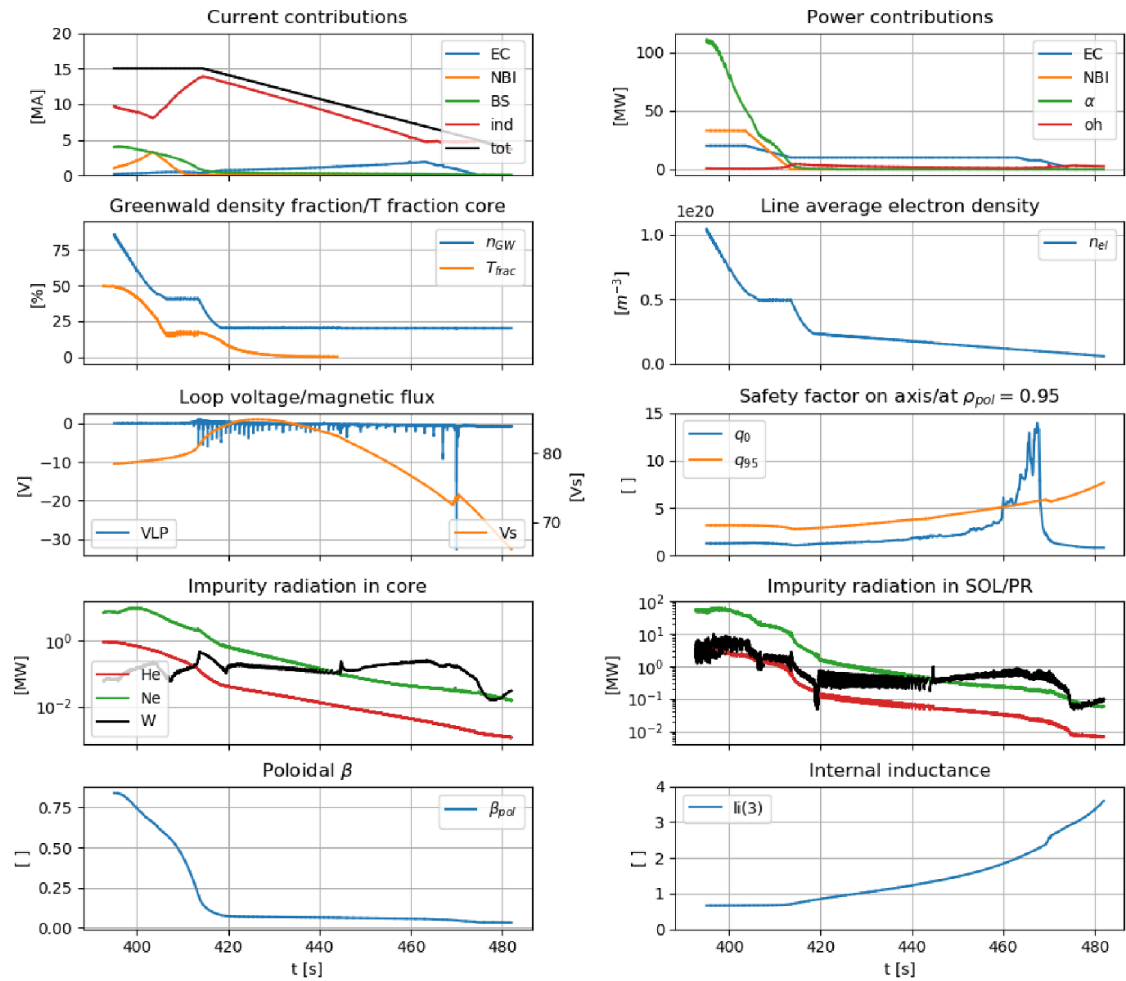


Figure 16. Time traces summarizing the exit phase starting from the flat-top burning phase at 395 s.

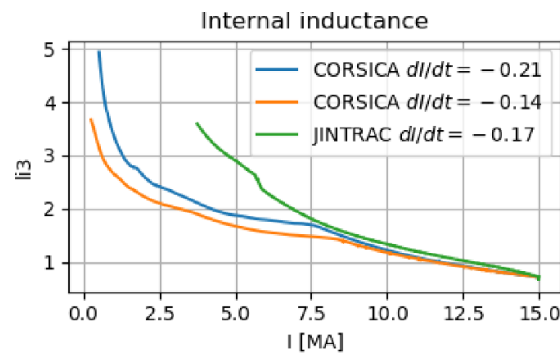


Figure 17. Internal inductance during the current ramp-down (green) compared to CORSICA simulations published in figure 16 of [42] taking into account vertical stability during the current ramp-down. Reproduced courtesy of IAEA. Figure from [42]. © 2018, ITER Organization.

remaining within operational limits. In this work, the full EC power is used in the range $\rho_r = 0.1 - 0.3$. The potential use of the central EC to stabilize tearing modes [47] or limit current holes is outside the scope of this paper.

Acknowledgments

JINTRAC was used under licence agreement between Euratom and CCFE, reference Ares (2014)3576010 — 28/10/2014. This work was part funded by the RCUK Energy Programme [Grant Number EP/T012250/1], EPSRC Energy Programme [Grant Number EP/W006839/1], and by ITER Task Agreement C19TD53FE implemented by Fusion for Energy under Grant GRT-869 and Contract OPE-1057. The views and opinions expressed herein do not necessarily reflect those of the ITER Organization. To obtain further information on the data and models underlying this paper please contact PublicationsManager@ukaea.uk.

Appendix. Core-Edge boundary coupling

When running JETTO and EDGE2D coupled in JINTRAC, the EDGE2D grid is constructed to extend a very short (\approx mm's) distance inside the separatrix, and the innermost grid surface is taken to define the plasma boundary for JETTO. There is no overlap of the edge and core domains, so consistency of the solution is attained through continuity of solution variables and fluxes at the core-edge interface. The fluid equations that are coupled across this boundary are the particle continuity equations for all ion charge states, the ion temperature (T_i) equation, and the electron temperature (T_e) equation. In JINTRAC zero parallel/toroidal velocity condition is enforced at the core-edge boundary surface, which decouples JETTO's toroidal momentum equation from EDGE2D parallel momentum equations. In addition, neutral fluxes crossing the core-edge boundary surface are exchanged to provide continuity for the separate source modelling components in the core and in the edge. Core-edge boundary conditions are always configured so that a flux condition is used by one code and a Dirichlet condition by the other. The code chosen to use a flux condition is the one which will generally receive a positive influx, as boundary conditions with outfluxes can lead to negative solutions and a Dirichlet condition is then the better option. This has resulted in the choices presented in table A1. The flux condition for EDGE2D at the core boundary is enforced by using a Dirichlet boundary condition where the value imposed is poloidally uniform and adjusted to generate the supplied flux. The impurity density of individual charge states may have strong poloidal dependence near the core boundary arising from the influence of temperature variations on the ionisation-recombination balance. Imposing the Dirichlet boundary condition uniformly at the core is contradictory and can give rise to unphysical and destabilising radial fluxes. Instead the density is distributed by evenly mixing in the poloidal distribution from the neighbouring ring.

Table A1. Boundary conditions.

Equation	EDGE2D	JETTO
n_i	Flux	Density
T_i	Flux	Temperature
T_e	Flux	Temperature
n_z	Density	Flux

ORCID iDs

F. Eriksson  <https://orcid.org/0000-0002-2740-7738>
 E. Tholerus  <https://orcid.org/0000-0002-3262-1958>
 D. Farina  <https://orcid.org/0000-0003-0795-3632>
 L. Figini  <https://orcid.org/0000-0002-0034-4028>
 L. Garzotti  <https://orcid.org/0000-0002-3796-9814>
 F. Koechl  <https://orcid.org/0000-0001-9706-6855>
 A. Loarte  <https://orcid.org/0000-0001-9592-1117>
 E. Militello Asp  <https://orcid.org/0000-0001-8183-8734>
 S.D. Pinches  <https://orcid.org/0000-0003-0132-945X>
 P. Strand  <https://orcid.org/0000-0002-8899-2598>

References

- [1] Romanelli M. et al 2014 *Plasma Fusion Res.* **9** 3403023
- [2] Koechl F. et al 2020 *Nucl. Fusion* **60** 066015
- [3] Militello Asp E. et al 2022 *Nucl. Fusion* **62** 126033
- [4] Garzotti L. et al 2019 *Nucl. Fusion* **59** 026006
- [5] Farina D. et al 2007 *Fusion Sci. Technol.* **52** 154
- [6] Strand P. et al 2004 *Proc. 31st EPS Conf. (London, UK)*
- [7] Harting D. et al 2016 *22nd PSI Conf. (Rome, Italy)*
- [8] Cenacchi G. and Taroni A. 1988 *Internal Report JET-IR(88)03* (available at: https://inis.iaea.org/collection/NCLCollectionStore/_Public/19/097/19097143.pdf)
- [9] Simonini R. et al 1994 *Contrib. Plasma Phys.* **34** 368
- [10] Reiter D. et al 2005 *Fusion Sci. Technol.* **47** 172
- [11] Baylor L.R. et al 2007 *Nucl. Fusion* **47** 443–8
- [12] Combs S.K. et al 2005 *Fusion Eng. Des.* **75** 691
- [13] Pégourié B. et al 2007 *Nucl. Fusion* **47** 44
- [14] Baylor L.R. et al 2016 *IEEE Trans. Plasma Sci.* **44** 9
- [15] Polevoi A.R. et al 2018 *Nucl. Fusion* **58** 056020
- [16] Kotov V. and Reiter D. 2009 *Plasma Physics Control. Fusion* **51** 115002
- [17] Tamor S. 1981 *J. Comput. Phys.* **40** 104
- [18] Summers H.P. 2001 The ADAS manual, version 2.3 (available at: www.adas.ac.uk)
- [19] Eckstein W. 1991 *Computer Simulation of Ion-Solid Interactions* (Springer)
- [20] Bateman G. 1980 Distribution of neutrals scattered off a wall *PPPL Appl. Phys. Rep.* **1**
- [21] Belo P. et al 2015 *42nd EPS Conf. on Plasma Physics (Lisbon, Portugal)*
- [22] Fichtmueller M. et al 1998 *Contrib. Plasma Phys.* **38** 284
- [23] Kaveeva E. et al 2020 *Nucl. Fusion* **60** 046019
- [24] ITER Organisation Report no. ITR-18-003 2018 *Internal Report* (ITER Organization, France) (available at: www.iter.org/technical-reports)
- [25] Challis C.D. et al 1989 *Nucl. Fusion* **29** 563–70
- [26] Kim S.H. et al 2009 *Plasma Physics Control. Fusion* **51** 105007
- [27] Koechl F. et al 2018 *Plasma Physics Control. Fusion* **60** 074008
- [28] Houlberg W.A. 1997 *Phys. Plasmas* **4** 3230
- [29] Erba M. et al 1997 *Plasma Phys. Control. Fusion* **39** 261
- [30] Fransson E. et al 2022 *Phys. Plasmas* **29** 112305

- [31] Parail V. et al 2009 *Nucl. Fusion* **49** 075030
- [32] Martin Y.R. et al 2008 *J. Phys.: Conf. Ser.* **123** 012033
- [33] Ryter F. et al 2014 *Nucl. Fusion* **54** 083003
- [34] Lukash V. et al 2005 *Plasma Devices Oper.* **13** 143–56
- [35] Khayrutdinov R.R. and Lukash V.E. 1993 *J. Comput. Phys.* **107** 106
- [36] Estrada-Mila C. et al 2006 *Phys. Plasmas* **13** 112303
- [37] Mikkelsen D.R. and Singer C.E. 1983 *Nucl. Tech. Fusion* **23** 4
- [38] Maruyama S. et al 2009 *23rd SOFE Conf.*
- [39] ITER Physics Basis Expert Groups on Confinement and Transport and Confinement Modelling and Database, ITER Physics Basis ed 1999 *Nucl. Fusion* **39** 2175
- [40] Gribov Y. et al 2016 *43rd EPS Conf. on Plasma Physics (Leuven, Belgium)*
- [41] Portone A. et al 2005 *Fusion Eng. Des.* **74** 537
- [42] Kim S.H. et al 2018 *Nucl. Fusion* **58** 056013
- [43] de Vries P.C. et al 2018 *Nucl. Fusion* **58** 026019
- [44] Kim S.H. et al 2023 *65th Annual Meeting of the APS Division of Plasma Physics (Denver, Colorado)*
- [45] Militello Asp E. et al 2023 First full plasma ITER integrated modelling studies with separated Deuterium and Tritium and optimal Tritium usage- Overview of JINTRAC simulations of the entire ITER 15MA/5.3T DT Q = 10 scenario *2023 IAEA Fusion Energy Conf.* p TH/7-1
- [46] Kim S.H. et al 2024 *Nucl. Fusion* **64** 016037
- [47] Poli F.M. et al 2018 *Nucl. Fusion* **58** 016007